Subscriber access provided by UNIV OF DURHAM

Article

# Sodium substitution in lead telluride

Xinke Wang, Igor Veremchuk, Matej Bobnar, Ulrich Burkhardt, Jing-Tai Zhao, and Yuri Grin

*Chem. Mater.*, **Just Accepted Manuscript** • DOI: 10.1021/acs.chemmater.7b05091 • Publication Date (Web): 29 Jan 2018

**Downloaded from http://pubs.acs.org on January 30, 2018**

**Just Accepted**

“Just Accepted” manuscripts have been peer-reviewed and accepted for publication. They are posted online prior to technical editing, formatting for publication and author proofing. The American Chemical Society provides “Just Accepted” as a free service to the research community to expedite the dissemination of scientific material as soon as possible after acceptance. “Just Accepted” manuscripts appear in full in PDF format accompanied by an HTML abstract. “Just Accepted” manuscripts have been fully peer reviewed, but should not be considered the official version of record. They are accessible to all readers and citable by the Digital Object Identifier (DOI®). “Just Accepted” is an optional service offered to authors. Therefore, the “Just Accepted” Web site may not include all articles that will be published in the journal. After a manuscript is technically edited and formatted, it will be removed from the “Just Accepted” Web site and published as an ASAP article. Note that technical editing may introduce minor changes to the manuscript text and/or graphics which could affect content, and all legal disclaimers and ethical guidelines that apply to the journal pertain. ACS cannot be held responsible for errors or consequences arising from the use of information contained in these “Just Accepted” manuscripts.

Chemistry of Materials is published by the American Chemical Society. 1155 Sixteenth Street N.W., Washington, DC 20036

Published by American Chemical Society. Copyright © American Chemical Society. However, no copyright claim is made to original U.S. Government works, or works produced by employees of any Commonwealth realm Crown government in the course of their duties.

# Sodium substitution in lead telluride

Xinke Wang,[1] Igor Veremchuk,[1] Matej Bobnar,[1] Ulrich Burkhardt,[1] Jing-Tai Zhao[2, 3] and Yuri Grin[1]*

[1]Max-Planck-Institut für Chemische Physik fester Stoffe, 01187 Dresden, Germany

[2]School of Materials Science and Engineering, Shanghai University, Shanghai 200444, China

[3]Nanophotonics Center, Texas Tech University, Lubbock, TX 79409, USA

**ABSTRACT:** Sodium is widely used as substituting element in *p*-type PbTe-based thermoelectric materials. In this work, two series of polycrystalline samples $Pb_{1-y}Na_yTe_{1-y/2}$ (total charge balance) and $Pb_{1-x}Na_xTe$ (total charge non-balance) were examined. Na has limited solubility for both of the series. The MAS $^{23}Na$ NMR analysis of $Pb_{1-x}Na_xTe$ series (for $Pb_{0.98}Na_{0.02}Te$ sample after SPS) reveals only one Na signal, corresponding to Na atoms coordinated by six Te atoms, indicating substitution of Pb by Na without defects in the Te sublattice. In the $Pb_{1-y}Na_yTe_{1-y/2}$ series, clustering of Na atoms with reduced coordination by Te was observed. Additional heat treatment of these samples leads to the reorganization of the Na-clusters in PbTe and their equilibration with the homogenized distribution of Na in the whole volume. The maximum *ZT* values of 1.4 ÷ 1.6 at 760 K are established for both $Pb_{1-x}Na_xTe$ and $Pb_{1-y}Na_yTe_{1-y/2}$ series. Upon long-time annealing at 873 K, reorganization and redistribution of Na atoms lead to the change in carrier concentration and, consequently, the thermoelectric properties for both series.

## Introduction

Thermoelectric materials have the ability to interconvert heat and electricity, which could play an important role in the alternative, environmentally friendly approach within the global sustainable energy solution.[1, 2] The efficiency of thermoelectric materials is quantified by the thermoelectric dimensionless figure of merit $ZT = \sigma S^2 T/(\kappa_{el}+\kappa_L)$, where $S$ is the Seebeck coefficient, $\sigma$ is the electrical conductivity, $\kappa_{el}$ is the electronic thermal conductivity, $\kappa_L$ is the lattice thermal conductivity and $T$ is the absolute temperature.[3-5] The rock-salt structured, narrow-band gap lead chalcogenides (PbX, X=Te, Se, S) semiconductors have been previously studied because of their outstanding thermoelectric performance.[6-14] Na has been proved as one of the most effective dopants in controlling hole-carriers concentration in PbX and therefore has been extensively utilized in order to optimize their thermoelectric properties.[15-19] Experimental and theoretical studies indicate that Na substitution will not introduce resonant levels in the electronic band structure of PbTe but, rather, move the Fermi surface close to the heavy-hole valence band.[18,20-21] Due to large mass and radii fluctuations, a reduced lattice thermal conductivity can also be achieved by Na substitution.[22-23] The Na-doped PbTe, called "2P-PbTe", has been used in 1959 RTG and for several NASA missions in the 1960's.[24-25] In 2011, Pei *et. al.* [15] re-evaluated the thermoelectric properties of *p*-type PbTe:Na using new reliable high-temperature thermal conductivity data. As a result, the maximum *ZT* ~ 1.4 was obtained, instead of the earlier underestimate of *ZT* = 0.7. Recently, progress has been made to obtain high *ZT* in Na-doped PbTe-based bulk materials using various substitutions (Mg, Ca, Sr, Ba, Hg, Cd, Yb, Mn).[26-35]

It is believed that the monovalent Na is substituting Pb. Typically Na is added to PbTe and PbTe-based materials in the form of NaTe or $Na_2Te$, thus giving rise to formation of acceptor centers.[15, 31, 36-40] First experiments revealed the diffusion coefficient increasing with increasing Na concentration. If Na diffuses *via* Pb vacancies, the respective diffusion coefficient would be expected to decrease. Such anomalous concentration dependence of the diffusion coefficient was explained by presence of the Te vacancies, which may indeed reduce the energy barriers for migration, temporarily making it possible for Na to reside on Te sites. In other words, the diffusion coefficient should increase with increasing Na concentration if Te vacancies take part in the diffusion mechanism.[17]

In a later study, the hole concentration was found to be considerably smaller than a value calculated from the amount of Na added to the reaction mixture, assuming one hole was produced per one Na atom. The maximum Na solubility in PbTe was experimentally determined to lie somewhere between 0.5 *at.* % and 1.75 *at.* %, although some loss of Na may occur during processing.[36, 39] The maximum observed carrier concentration is 2.5 × $10^{20}$ $cm^{-3}$. Each Na atom donates about one hole when Na concentration is higher than ~ 6 × $10^{19}$ $cm^{-3}$, which corresponds to 0.84 *at.* %.[16] However, at Na concentration less than this value, one hole produced by two Na atoms was distinguished experimentally. For the nature of the acceptor centers at small Na concentrations, a proposed model implies a formation of the significant complex center $(\mathrm{Na_{Pb}}\square_{\mathrm{Te}}\mathrm{Na_{Pb}})$.[16]

The systematic study of PbTe-$Na_2Te$ and PbTe-NaTe quasi-binary phase diagrams shows that only $Na_2Te$ (anti-$CaF_2$ crystal structure[40]) and NaTe phase (own molecular-like structure[41]) are found in these systems.[42] According to the chemical analysis by electron microprobe WDS, the maximum solubility of Na in PbTe was found to be 1.4 ± 0.3 mol % (0.7 *at.* % Na average values from more than 100 point analysis) at 623 K. While at 513 K, the solubility value decreases to 0.24 ± 0.14 *at.* %.[39] First-principles calculations of defect energy in Na-Pb-Te indicate that Na substituting Pb is the lowest-energy defect ($\mathrm{Na_{Pb}}^{1-}$); here the solubility should increase with increasing temperature.[37] In recent microscopic studies on Na-doped polycrystalline PbTe samples, Na-rich nano-segregations at mesoscale imperfections, dislocations, and grain boundaries even nanoscale precipitates were formed beyond the solubility limit,[43-45] which may provide additional scattering centers and reduce the thermal conductivity[36, 46] or increase the high-temperature electrical conductivity due to re-dissolution of Na at elevated temperatures.[44] However, simple 1:1 substitution Pb by Na is mostly considered in the experimental studies. The complete shape of the solid solution of Na in PbTe within the ternary system Na-Pb-Te was not established (cf. Ref. 39). As a consequence, the influence of different Pb-by-Na substitution mechanisms on the thermoelectric activity of the ternary materials remains unclear. The possibility of the two substitution schemes is indicated or assumed by different Na-additives (NaTe or $Na_2Te$) for formation of acceptor centers. In a freshly appeared work, the n-type materials were rather unexpectedly obtained by ball milling of PbTe with $Na_2Te$.[47]

In this report, the crystal structure features and thermoelectric properties of samples series $Pb_{1-y}Na_yTe_{1-y/2}$ (total charge balance) and $Pb_{1-x}Na_xTe$ (total charge non-balance) have been investigated in order to achieve deeper understanding of the Na substitution in PbTe.

## Experimental details

Bulk polycrystalline samples $Pb_{1-x}Na_xTe$ ($0 \le x \le 0.04$), $Pb_{1-y}Na_yTe_{1-y/2}$ ($0 \le y \le 0.10$), were synthesized by melting the elements Pb (shot, 99.999 mass %), Te (chunk, 99.9999 mass %), Na (chunk, 99.99%) in a graphite-coated and fused silica tube at 1273 K for 6 h under a vacuum of around $10^{-4}$ torr. Then, the temperature was slowly lowered to 873 K and the samples were annealed for six days for homogenization. The obtained ingots were ground into powders by hand using an agate mortar in an argon atmosphere before spark-plasma sintering (Fuji SPS-515S) at 673 K under a pressure of 60 MPa for 7 minutes. The polished SPS-manufactured disks (∅ = 10 mm, 2 mm thick) were first used for measurements of the thermal diffusivity. Then the disks were cut into rectangular blocks ($2 \times 2 \times 8$ mm$^3$) by wire saw in order to obtain specimens for measurements of electrical resistivity and Seebeck coefficient. The cut sample bars were sealed in Ta tubes under Ar atmosphere in fused silica tube for annealing at 873 K, with following quenching in ice water after 900 hours. $Na_2Te$, for the NMR investigations, was synthesized by melting Na and Te in the stoichiometric ratio in an Ar atmosphere in a sealed Ta tube at 773 K for 5 hours.

Phase identification was performed with the X-ray Guinier diffraction technique (Huber G670 camera, Cu $K_{\alpha 1}$ radiation, $\lambda = 1.54056$ Å, $\Delta 2\theta = 0.005°$, $2\theta$ range 3.0° - 100°, exposure time 6×15 min). The reflection positions, obtained by profile deconvolution, were corrected using the internal standard $LaB_6$. Lattice parameter refinements and other crystallographic calculations were performed with the program package WinCSD.[48]

For the metallographic study, the materials pieces were embedded in conductive resin, subsequently grinded and polished. The sample homogeneity was examined by optical microscopy (Zeiss Axioplan2) in bright-field and polarized light. The element mappings were obtained by electron microprobe analysis with the energy dispersive X-ray spectroscopy (Bruker Quantax 400 system with the detector XFlash 630) on the polished bulk materials. Elemental chemical analysis (for Pb, Te, Na, O) was performed by using the inductively-coupled plasma optical-emission spectrometry (ICP-OES, Agilent 5100 SVDV setup for Pb, Te, Na) and the carrier-gas hot-extraction technique (LECO TCH600 setup for oxygen).

Electrical resistivity and Seebeck coefficient were measured simultaneously with the ZEM-3 setup (Ulvac-Riko) in the temperature range 300 to 760 K. The Hall effect ($R_H$) was measured with a standard four-point *ac* technique in a physical property measurement system (PPMS, Quantum Design), with magnetic fields up to 9 T. The Hall carrier concentrations were calculated by $1 / (R_H \cdot e)$, where $R_H$ is Hall coefficient, $e$ is the electron charge. Thermal diffusivity ($D$) measurements were conducted with the Netzsch LFA 457 equipment (LFA). The heat capacity per atom ($C_p$) was estimated from the relation $C_p / k_B = 3.07 + 0.00047(T - 300)$[49]. Thermal conductivity was calculated as $\kappa = dC_pD$, where $d$ is the density obtained using the mass and the geometric volume of the specimen disk after SPS. Lattice thermal conductivity ($\kappa_L$) was calculated by subtracting the electronic part $\kappa_e = L\sigma T$ (the Wiedemann-Franz law) from the total conductivity, the Lorenz number is evaluated from the equation: $L = 1.5 + \exp[-\frac{|S|}{116}]$, which is accurate within 20% for PbTe.[50]

Nuclear Magnetic Resonance (NMR) experiments were performed on a Bruker Avance 500 spectrometer with a magnetic field of $B_0 = 11.74$ T and standard Bruker MAS probes. The samples were diluted with $GeO_2$ and packed into 4 mm $ZrO_2$ rotors. The $^{23}$Na signals were referenced to saturated solution of NaCl with the reference frequency of 132.29127 MHz. The spectra were obtained either from the free induction decay after a single pulse of 2 μs or from the echoes after two 90° pulses of 6 μs. The recovery time was 10 s. The experiments were performed under static and spinning conditions with the spinning rates provided in the text below.

## Results and discussion

We prepared two series of the samples (Figure 1a, top). The first series with the nominal composition $Pb_{1-x}Na_xTe$ ($x$ = 0.005 ÷ 0.04) assumes that Na atoms simply substitute Pb. All as-cast samples are single-phase materials according to the powder X-ray diffraction (PXRD). The lattice parameters decrease with the increasing Na concentration monotonically up to 1 *at.*% (Figure 1b, red squares) being in accord with the respective ionic radii of the $Na^+$ (0.99 Å) and $Pb^{2+}$ (1.19 Å).[22] This signalizes the homogeneity range border in direction to the NaTe phase of about 1 *at.*% of Na, being well in agreement with the results obtained at 623 K.[39] Relatively small value of Na concentration can be understood given a strong difference in the crystal structure: ionic NaCl-type structure of PbTe *vs.* Te polyanions in NaTe (Figure 1a). Above 1 *at.* %, the gradient of lattice parameter changes, but it is not zero as expected for the samples in the multiphase region. This observation may indicate a non-complete homogeneity of the material after the primary heat treatment. After additional SPS treatment (at $T$ = 673 K), the lattice parameters of the cubic phase for $x > 1$ *at.* % remain unchanged within 2 e.s.d. (Figure 1b, red triangles), confirming the border of the homogeneity range. The samples may still not be completely homogeneous, which is also revealed by the measurements of thermoelectric properties (see below). The inhomogeneity of the samples can arise on the atomic level, since DTA (Figure 2) and element mapping scanning (Figure 3) experiments do not reveal any presence of additional phases, phase transformations, etc. The only exception are small Na-rich agglomeration areas in the microstructures (Figure 3). The absolute values of the lattice parameters are slightly reduced after the SPS treatment, caused by further ordering in the crystal structure due to the enhanced diffusion under SPS conditions. During thermoelectric measurements, some Na was lost (Table S1), and the lattice parameters are becoming slightly larger for each sample (Figure 1b, red stars).

For the $Pb_{1-y}Na_yTe_{1-y/2}$ series ($y$ = 0.005 ÷ 0.10, Figure 1a, b), the change of the lattice parameters with the substitution is not as strong as in the previous case. This is understandable assuming that the reduction of the lattice parameters due to the ionic radii of $Pb^{2+}$ and $Na^{1+}$ is partially compensated by the repulsive interaction of the cations around the Te defect. After thermoelectric measurement, the monotonic slope of lattice parameter is observed up to 2.5 *at.* % of Na toward the $Na_2Te$ phase (Figure 1b) which is possible to understand given the structural similarity of PbTe (NaCl type) and $Na_2Te$ (anti-$CaF_2$ type). The relative changes of the lattice parameter for the $Pb_{1-y}Na_yTe_{1-y/2}$ samples are similar to that of the $Pb_{1-x}Na_xTe$ series, with the increasing Na content. However, depending on heat treatment, there is an opposite lattice parameter change in these two series. In the case of $Pb_{1-x}Na_xTe$, it increases after LFA measurement, as opposed to $Pb_{1-y}Na_yTe_{1-y/2}$ samples, for which the lattice parameter decreases. After annealing, the lattice parameter of both $Pb_{1-y}Na_yTe_{1-y/2}$ and $Pb_{1-x}Na_xTe$ series obeys Vegard's law and this trend is more prominent for the samples before annealing (Figure 1b). In case of $Pb_{1-y}Na_yTe_{1-y/2}$, the maximum solubility of Na is 1.5 *at.* %, in contrast to 2.5 *at.* % before annealing; and for $Pb_{1-x}Na_xTe$, 0.5 *at.* % as compared to 1.0 *at.* %.

This complex behavior of Na substitution raises the question of where in the crystal structure Na is located. Because the X-ray powder diffraction cannot yield this information, the NMR spectroscopy was performed. Figure 4 shows the MAS $^{23}Na$ NMR spectra of the selected samples from the $Pb_{1-y}Na_yTe_{1-y/2}$ and the $Pb_{1-x}Na_xTe$ series. The MAS $^{23}Na$ NMR spectrum of $Pb_{0.98}Na_{0.02}Te$ after SPS (shown in black in Figure 4, bottom) shows one strong peak at about -14 ppm. Because there is no evidence for another phase(s) in this sample, and the Pb-by-Na substitution is the most probable case, the peak at -14 ppm should come from Na replacing Pb in the PbTe. The Na atom is coordinated by six Te atoms (Figure 4, top right) and according to Ref. 51, the higher coordination of Na atoms by negatively charged atoms results in more negative chemical shifts. The MAS $^{23}Na$ NMR spectrum of the as cast sample $Pb_{0.95}Na_{0.05}Te_{0.975}$ is more complex (orange line, Figure 4 bottom). The weak peak at -13 ppm corresponds to the main peak of the $Pb_{0.98}Na_{0.02}Te$ samples, thus it is assigned to Na replacing Pb in the PbTe structure. The main peak at +40.6 ppm corresponds to more complex arrangement of the Na atoms in the structure, the same signal is also observed in as-cast $Pb_{0.98}Na_{0.02}Te$ (Figure 4, blue spectra), which disappeared after additional heat treatment (Figure 4, black spectra).The ratio of its intensity (including all its sidebands) to the negatively shifted peak is approximately 6:1.

The position and assignment of this effect is evaluated by comparison to the spectrum of the binary compound $Na_2Te$. We synthesized it and performed the NMR experiment. The $^{23}Na$ NMR signal has practically the same position at +40.7 ppm (Figure S1). However, the MAS line of $Na_2Te$ is significantly narrower (FWHM of 0.5 ppm compared to FWHM of 2.8 ppm for $Pb_{0.95}Na_{0.05}Te_{0.975}$). The broader line for the $Pb_{0.95}Na_{0.05}Te_{0.975}$ sample points toward the disorder in the crystal structure being in agreement with the behaviour of the lattice parameters (Figure 1a). The relatively large positive value of chemical shift is in accordance with Na being four-coordinated by Te in $Na_2Te$.[51] Thus the signal at +40.7 ppm in the spectrum of $Pb_{0.95}Na_{0.05}Te_{0.975}$ is assigned to Na atoms replacing Pb in vicinity of the Te vacancy. The larger shift and the large relative intensity of the main signal can be understood assuming the clustering of the Na atoms around the Te defect in order to reduce the local excess charge appearing by the vacancy formation (Figure 4, top left). All these observations echo with the Crocker's idea about formation of the significant complex center $(Na_{Pb}\square_{Te}Na_{Pb})$.[16]

Even small concentration of the Na improves the metallic behavior for all samples in comparison to the binary PbTe, which is characterized by the metal–semiconductor transition[14] (Figure 5). All Hall measurements were conducted after SPS treatment and thermal diffusivity measurements. The Hall carrier concentration of $Pb_{1-x}Na_xTe$ and $Pb_{1-y}Na_yTe_{1-y/2}$ decreases with increasing temperature, the values obtained at 300 K are roughly two times smaller than those at 50 K for all samples (Figure 5a). Similar behavior is observed for hole mobility values (Figure 5b). For both substitution series, the carrier concentration is smoothly increasing with the Na content within the homogeneity range of the solid solution. According to the assumption, that one $Na^+$ donates one hole, we calculate the theoretical carrier concentrations for the $Pb_{1-x}Na_xTe$ series (Figure 5a). The measured values of Hall charge carrier concentration correspond to 60 ~ 70 % or less of the calculated one (Figure 5a), which suggests that a simple chemical one-charge model is not in complete agreement with the band structure of these materials. This conclusion is further supported by the behavior of the $Pb_{1-y}Na_yTe_{1-y/2}$ series. Here, for the charge balance situation, the mutual compensation between Na holes and Te defects can be assumed, so the number of charge carriers should not be directly dependent on $y$. The presence of such dependence in Figure 5a can be explained by the fact that a part of substituting Na atoms follows the behavior in the $Pb_{1-x}Na_xTe$ (cf. NMR results in Figure 4). Additional explanation is the appearance of new states in the band structure, caused by the environment of the Te vacancies.

All samples of both series are *p*-type conductors (Figure 6), in contrast to the binary PbTe, which shows a *p-n* transition with temperature. The specimens of the $Pb_{1-y}Na_yTe_{1-y/2}$ series show similar conductive behavior for the whole temperature range. The Seebeck coefficient values at 300 K are comparable to the materials of the $Pb_{1-x}Na_xTe$ series, which is consistent with experimental charge carrier concentrations (Figure 5). Upon increasing of Na content, the resistivity decreases up until $y \geq 0.03$, the electronic transport properties of $Pb_{1-y}Na_yTe_{1-y/2}$ samples do not change significantly ($x \geq 0.02$ for $Pb_{1-x}Na_xTe$ samples). An exception is the $y = 0.10$ sample, for which a formation of the secondary phase is observed. Room temperature values of Seebeck coefficient $S$ as a function of the Hall carrier concentration for all studied samples are consistent with the published data for PbTe:Na[15, 31, 33] (Figure 7a). However, the carrier mobility values for all studied samples are much lower compared to the published PbTe:Na data[15, 31, 33], but higher than that for PbTe:Tl[13, 28, 52] (Figure 7b).

The total and lattice thermal conductivities of the $Pb_{1-x}Na_xTe$ samples show smaller values compared to that of $Pb_{1-y}Na_yTe_{1-y/2}$ (Figure 8). Generally, lattice thermal conductivity decreases with Na concentration for all samples, especially for the high temperature range. Therefore, the maximum $ZT$ values are around 1.4 ~ 1.6 at 760 K for $Pb_{1-x}Na_xTe$ ($x \geq 0.02$) and $Pb_{1-y}Na_yTe_{1-y/2}$ ($0.1 \geq y \geq 0.03$, Figure 9), comparable with previous results.[15] Within the homogeneity range of the solid solution, the decrease of the lattice and total thermal conductivity goes along with the increasing local structural disorder according to the substitution schemes above. In the multi-phase samples, the additional phonon scattering on the phase boundaries reduces further the total thermal conductivity.

Although both series of materials show high values of $ZT$, they degrade during the measurement. The samples of $Pb_{1-y}Na_yTe_{1-y/2}$ oxidized slightly, especially those with high Na concentration ($y \geq 0.03$). During the cyclic thermal conductivity measurements, the samples of $Pb_{1-x}Na_xTe$ ($x \geq 0.02$) show obvious change between the first heating cycle and the following ones, whereas no such effect was found in $Pb_{1-y}Na_yTe_{1-y/2}$, even for the highest Na concentration outside the homogeneity range ($Pb_{0.90}Na_{0.10}Te_{0.95}$). For example, the thermal conductivity of samples with $x$ and $y$ of 0.04 (Figure 10) during the first heating cycle for both samples are almost the same until 650 K, while at higher temperature, the thermal conductivity of $Pb_{0.96}Na_{0.04}Te$ shows jump-like decrease, in contrast to the $Pb_{0.96}Na_{0.04}Te_{0.98}$. The cooling and all following measurements yield stable, but lower values, as compared to the initial heating curve (Figure 10). After full cycle measurements, including electrical and Seebeck coefficient, the $Pb_{0.96}Na_{0.04}Te$ material shows visible microscopic cracks or voids and is partially deformed (cf. inset of Figure 10). Contrary to this, sample of $Pb_{0.96}Na_{0.04}Te_{0.98}$ did not show any obvious microscopic changes.

In order to evaluate the possibility of these materials in potential application in thermoelectric modules, further characterization of the thermal stability for samples annealed at 873 K for 900 hours were carried out. The chemical composition, lattice parameters, and carrier concentrations of the selected samples are presented in Table S2. As mentioned above, the solubility of Na is decreased according to the evolution of the lattice parameters, which is likely due to reorganization of Na clusters since no Na loss after annealing was observed in the chemical analysis (Table S2). The $^{23}Na$ MAS NMR investigations of the annealed $Pb_{0.95}Na_{0.05}Te_{0.975}$ sample (green spectra in Figure 4) reveal that the ratio between the two main peaks has changed. The intensity of the peak, which is assigned to Na replacing Pb in the PbTe, is much higher as compared to the peak corresponding to a clustering of the Na atoms around the Te defect. A heat treatment leads to an equilibration and homogenisation of the samples by reorganization and distribution of the Na clusters and Te vacancies. From the powder XRD and chemical analyses, the maximum solubility of Na is: ~1.0 *at.* % (corresponding to 1.5 *at.* % nominal Na content. Na loss took place during the measurements) for $Pb_{1-y}Na_yTe_{1-y/2}$ sample series and 0.5 *at.* % for $Pb_{1-x}Na_xTe$ (Figure 1c). After annealing, the resistivity shows higher values for all samples, especially for the high temperature range (Figure 11), which can be attributed the reduced carrier concentration. The resistivity and Seebeck coefficient values do not change significantly for $Pb_{1-x}Na_xTe$ ($x \geq 0.01$) and for $Pb_{1-y}Na_yTe_{1-y/2}$ ($y \geq 0.03$), as evident from Figure 11. This is consistent with the change of the lattice parameters. The power factors of $Pb_{1-x}Na_xTe$ samples are very similar with before annealing, especially at high temperature range (Figure 12). However, all $Pb_{1-y}Na_yTe_{1-y/2}$ samples show a significant reduction of the power factors at high temperature range after annealing (Figure 12). As a result, the calculated $ZT$ values (using same thermal conductivity values as those measured before annealing) of the annealed $Pb_{1-x}Na_xTe$ samples are still very high, but somewhat reduced for the annealed $Pb_{1-y}Na_yTe_{1-y/2}$ samples (Figure 13).

## Conclusions

Two different substitution schemes $Pb_{1-x}Na_xTe$ (known one) and $Pb_{1-y}Na_yTe_{1-y/2}$ (new one) were systemically investigated, and the shape of the solid solution of Na in PbTe in the ternary system Na-Pb-Te was established. Na has limited while different solubility range for each series: 1.0 *at.* % for $Pb_{1-x}Na_xTe$, and 2.5 *at.* % for $Pb_{1-y}Na_yTe_{1-y/2}$. The samples with high concentration of Na ($x \geq 0.02$ in $Pb_{1-x}Na_xTe$) showed a jump-like behavior above 650 K during the first heating cycle, which becomes stable and achieves lower values in further cyclic measurements. However, thermal conductivities of $Pb_{1-y}Na_yTe_{1-y/2}$ samples are stable during the measurements.

The local atomic arrangement by different substitution schemes were revealed by NMR. The MAS $^{23}Na$ NMR of the $Pb_{0.98}Na_{0.02}Te$ after SPS revealed only one Na signal, which is assigned to Na replacing Pb in the PbTe. This peak had much lower intensity in the sample of $Pb_{0.95}Na_{0.05}Te_{0.975}$, however, an additional strong peak was observed, which was assigned to Na atoms replacing Pb in vicinity of the Te vacancy. The larger shift and the large relative intensity of the main signal can be understood assuming the clustering of the Na atoms around the Te defect. This suggestion is consistent with Crocker's idea about formation of acceptor center $Na_{Pb}\square_{Te}Na_{Pb}$ in PbTe[16] and formation of the Na-rich nano-segregations or nanoscale precipitates.[43-44,46] Moreover, those Na-aggregation structures may also be responsible for the less than 100% doping efficiency from Pb-by-Na substitution. A long-term heat treatment leads to an equilibration and homogenisation of the samples by reorganization and distribution of the Na clusters and Te vacancies. Concerning powder XRD analysis, the maximum solubility of Na is reduced upon annealing for both sample series: ~1.0 *at.* % for $Pb_{1-y}Na_yTe_{1-y/2}$ and 0.5 *at.* % for $Pb_{1-x}Na_xTe$.

The thermoelectric properties of the single-phase materials were proved to be different by different substitution schemes. The maximum *ZT* values of 1.4 ÷ 1.6 at 760 K are established for both $Pb_{1-x}Na_xTe$ ($x \geq 0.02$) and $Pb_{1-y}Na_yTe_{1-y/2}$ ($0.1 \geq y \geq 0.03$) series in the multi-phase samples due to the additional reduction of the thermal conductivity on the phase boundaries. $Pb_{1-x}Na_xTe$ substitution series exhibit better thermoelectric properties after long-time annealing. The degradation of thermoelectric properties by thermal annealing is proven experimentally.

## ASSOCIATED CONTENT

**Supporting Information**.

Chemical compositions and lattice parameters of the synthesized samples; comparison of compositions, lattice parameters and carrier concentrations before and after annealing; MAS $^{23}Na$ NMR spectra of $Pb_{0.95}Na_{0.05}Te_{0.975}$ (before SPS) and $Na_2Te$.

The Supporting Information is available free of charge on the ACS Publications website at DOI ...

## AUTHOR INFORMATION

### Corresponding Author

* E-Mail: grin@cpfs.mpg.de

### ORCID

Yuri Grin: 0000-0003-3891-9584

### Author Contributions

Y.G. and J.T.Z. designed the project, X.W. prepared the samples, X.W. and I.V. measured thermoelectric properties, M.B. performed NMR and Hall measurements, X.W. and U.B. performed metallographic experiments.

The manuscript was written through contributions of all authors. All authors have given approval to the final version of the manuscript.

### Funding

This research was partially supported by National Natural Science Foundation of China, Science and Technology Commission of Shanghai Municipality, State Administration of Foreign Experts Affairs.

### Notes

The authors declare no competing financial interest.

## ACKNOWLEDGMENT

Authors thank Dr. Marcus Schmidt (MPI CPfS) for DSC-TG measurements, Dr. Gudrun Auffermann (MPI CPfS) for chemical analysis, structure group of MPI CPfS for the powder XRD measurements, Dr. Eteri Svanidze for valuable discussion. Prof. Dr. Zhao thanks the support of the National Natural Science Foundation of China under Project No. 21771123, Science and Technology Commission of Shanghai Municipality under Project No. 15DZ2260300, and State Administration of Foreign Experts Affairs under project No. D16002.

## FIGURE CAPTIONS

**Figure 1.** (a) Phase diagram for Na-substituted PbTe samples. (b) Lattice parameter *vs.* nominal Na composition for the $Pb_{1-x}Na_xTe$ (red) and $Pb_{1-y}Na_yTe_{1-y/2}$ (black) series. For comparison, lattice parameter of the binary PbTe is shown[14] as a blue dash dot line. (c) Lattice parameter of annealed Na-substituted PbTe samples.

**Figure 2.** (a) TG / DTA measurement of $Pb_{0.98}Na_{0.02}Te$ after SPS; (b) DSC measurement of $Pb_{0.98}Na_{0.02}Te_{0.99}$ after SPS.

**Figure 3.** Back-scattered electrons (BSE) image (a) and element mapping of $Pb_{0.98}Na_{0.02}Te$ sample after SPS for (b) Na (K line), (c) Te (L lines), (c) Pb (M line).

**Figure 4**. Magic Angle Spinning (MAS) $^{23}Na$ NMR spectra of PbTe substituted with Na: (orange) $Pb_{0.95}Na_{0.05}Te_{0.975}$ after synthesis (before SPS); (blue) $Pb_{0.98}Na_{0.02}Te$ after synthesis (before SPS); (black) $Pb_{0.98}Na_{0.02}Te$ after SPS; (green) $Pb_{0.95}Na_{0.05}Te_{0.975}$ after 900 hours annealing. The spinning rate was 4.5 kHz. Spinning sidebands from the left and right signals are marked by asterisks and crosses, respectively.

**Figure 5.** (a) Hall carrier concentrations and (b) carrier mobility of $Pb_{1-x}Na_xTe$ (triangles) and $Pb_{1-y}Na_yTe_{1-y/2}$ (circles) at 50 K (blue) and at 300 K (red). The calculated values (green squares) assuming one $Na^+$ donates one hole.

**Figure 6.** Temperature dependences of (a) electrical resistivity, (b) Seebeck coefficient for $Pb_{1-x}Na_xTe$ and (c) electrical resistivity, (d) Seebeck coefficient for $Pb_{1-y}Na_yTe_{1-y/2}$.

**Figure 7.** (a) Room-temperature Seebeck coefficient as a function of Hall carrier concentration *n* and (b) room-temperature Hall mobility $\mu$ as a function of Hall carrier concentration *n* for $Pb_{1-x}Na_xTe$ (triangles), $Pb_{1-y}Na_yTe_{1-y/2}$ (circles). The black and the orange lines are literature data for PbTe: Na[15, 31, 33] and PbTe: Tl[13, 28, 52], respectively.

**Figure 8.** Temperature dependence of total and lattice thermal conductivity for $Pb_{1-x}Na_xTe$ (a, b) and $Pb_{1-y}Na_yTe_{1-y/2}$ (c, d).

**Figure 9.** Temperature dependence of the thermoelectric figure of merit *ZT* for (a) $Pb_{1-x}Na_xTe$ and (b) $Pb_{1-y}Na_yTe_{1-y/2}$.

**Figure 10.** Cyclic measurements of thermal conductivity for $Pb_{0.96}Na_{0.04}Te$ and $Pb_{0.96}Na_{0.04}Te_{0.98}$. Inset: image of $Pb_{0.96}Na_{0.04}Te$ (top) and $Pb_{0.96}Na_{0.04}Te_{0.98}$ (bottom) specimens after measurement.

**Figure 11.** Temperature dependences of electrical resistivity and Seebeck coefficient for $Pb_{1-x}Na_xTe$ after 900 hours annealing at 873 K (a, b) and $Pb_{1-y}Na_yTe_{1-y/2}$ after 900 hours annealing at 873K (c, d).

**Figure 12.** Temperature dependences of power factor for $Pb_{1-x}Na_xTe$ before (a) and after (b) 900 hours annealing at 873 K and for $Pb_{1-y}Na_yTe_{1-y/2}$ before (c) and after (d) 900 hours annealing at 873 K.

**Figure 13.** Temperature dependent of the thermoelectric figure of merit *ZT* for (a) $Pb_{1-x}Na_xTe$ and for (b) $Pb_{1-y}Na_yTe_{1-y/2}$ after 900 hours annealing at 873 K.

## REFERENCES

(1) Tan, G.; Zhao, L.-D.; Kanatzidis, M. G., Rationally Designing High-Performance Bulk Thermoelectric Materials. *Chem. Rev.* **2016,** *116* (19), 12123-12149.

(2) Zhang, Q. H.; Huang, X. Y.; Bai, S. Q.; Shi, X.; Uher, C.; Chen, L. D., Thermoelectric Devices for Power Generation: Recent Progress and Future Challenges. *Adv. Eng. Mater.* **2016,** *18* (2), 194-213.

(3) Sootsman, J. R.; Chung, D. Y.; Kanatzidis, M. G., New and Old Concepts in Thermoelectric Materials. *Angew. Chem., Int. Ed.* **2009,** *48* (46), 8616-8639.

(4) Snyder, G. J.; Toberer, E. S., Complex thermoelectric materials. *Nat. Mater.* **2008,** *7* (2), 105-114.

(5) Grebenkemper, J. H.; Hu, Y.; Barrett, D.; Gogna, P.; Huang, C.-K.; Bux, S. K.; Kauzlarich, S. M., High Temperature Thermoelectric Properties of $Yb_{14}MnSb_{11}$ Prepared from Reaction of MnSb with the Elements. *Chem. Mater.* **2015,** *27* (16), 5791-5798.

(6) Ravich, Y. I.; Efimova, B. A.; Smirnov, I. A., *Semiconducting Lead Chalcogenides*. Plenum Press: 1970.

(7) Wang, H.; Pei, Y. Z.; LaLonde, A. D.; Snyder, G. J., Heavily Doped *p*-Type PbSe with High Thermoelectric Performance: An Alternative for PbTe. *Adv. Mater.* **2011,** *23* (11), 1366-1370.

(8) Korkosz, R. J.; Chasapis, T. C.; Lo, S.-h.; Doak, J. W.; Kim, Y. J.; Wu, C.-I.; Hatzikraniotis, E.; Hogan, T. P.; Seidman, D. N.; Wolverton, C.; Dravid, V. P.; Kanatzidis, M. G., High ZT in *p*-Type $(PbTe)_{(1-2x)}(PbSe)_{(x)}(PbS)_{(x)}$ Thermoelectric Materials. *J. Am. Chem. Soc.* **2014,** *136* (8), 3225-3237.

(9) Lee, Y.; Lo, S.-H.; Androulakis, J.; Wu, C.-I.; Zhao, L.-D.; Chung, D.-Y.; Hogan, T. P.; Dravid, V. P.; Kanatzidis, M. G., High-Performance Tellurium-Free Thermoelectrics: All-Scale Hierarchical Structuring of *p*-Type PbSe-MSe Systems (M = Ca, Sr, Ba). *J. Am. Chem. Soc.* **2013,** *135* (13), 5152-5160.

(10) Zhang, Q.; Cao, F.; Liu, W.; Lukas, K.; Yu, B.; Chen, S.; Opeil, C.; Broido, D.; Chen, G.; Ren, Z., Heavy Doping and Band Engineering by Potassium to Improve the Thermoelectric Figure of Merit in *p*-Type PbTe, PbSe, and $PbTe_{1-y}Se_y$. *J. Am. Chem. Soc.* **2012,** *134* (24), 10031-10038.

(11) Wu, H. J.; Zhao, L. D.; Zheng, F. S.; Wu, D.; Pei, Y. L.; Tong, X.; Kanatzidis, M. G.; He, J. Q., Broad temperature plateau for thermoelectric figure of merit ZT > 2 in phase-separated $PbTe_{0.7}S_{0.3}$. *Nat. Commun.* **2014,** 5, 1-9.

(12) Pei, Y. Z.; Shi, X. Y.; LaLonde, A.; Wang, H.; Chen, L. D.; Snyder, G. J., Convergence of electronic bands for high performance bulk thermoelectrics. *Nature* **2011,** *473*, 66-69.

(13) Heremans, J. P.; Jovovic, V.; Toberer, E. S.; Saramat, A.; Kurosaki, K.; Charoenphakdee, A.; Yamanaka, S.; Snyder, G. J., Enhancement of thermoelectric efficiency in PbTe by distortion of the electronic density of states. *Science* **2008,** *321*, 554-557.

(14) Wang, X.-K.; Veremchuk, I.; Bobnar, M.; Zhao, J.-T.; Grin, Y., Solid solution $Pb_{1-x}Eu_xTe$: constitution and thermoelectric behavior. *Inorg. Chem. Front.* **2016,** *3* (9), 1152-1159.

(15) Pei, Y. Z.; LaLonde, A.; Iwanaga, S.; Snyder, G. J., High thermoelectric figure of merit in heavy hole dominated PbTe. *Energy Environ. Sci.* **2011,** *4* (6), 2085-2089.

(16) Crocker, A. J., The role of sodium in lead telluride. *J. Phys. Chem. Solids* **1967,** *28* (10), 1903.

(17) Crocker, A. J.; Dorning, B. F., Diffusion of sodium in lead telluride. *J. Phys. Chem. Solids* **1968,** *29* (1), 155.

(18) Ahmad, S.; Mahanti, S. D.; Hoang, K.; Kanatzidis, M. G., Ab initio studies of the electronic structure of defects in PbTe. *Phys. Rev. B* **2006,** *74* (15), 155205.

(19) Hoang, K.; Mahanti, S. D.; Kanatzidis, M. G., Impurity clustering and impurity-induced bands in PbTe-, SnTe-, and GeTe-based bulk thermoelectrics. *Phys. Rev. B* **2010,** *81* (11), 113709.

(20) Androulakis, J.; Todorov, I.; Chung, D. Y.; Ballikaya, S.; Wang, G. Y.; Uher, C.; Kanatzidis, M., Thermoelectric enhancement in PbTe with K or Na codoping from tuning the interaction of the light- and heavy-hole valence bands. *Phys. Rev. B* **2010,** *82* (11), 115209.

(21) Giraldo-Gallo, P.; Sangiorgio, B.; Walmsley, P.; Silverstein, H. J.; Fechner, M.; Riggs, S. C.; Geballe, T. H.; Spaldin, N. A.; Fisher, I. R., Fermi surface evolution of Na-doped PbTe studied through density functional theory calculations and Shubnikov-de Haas measurements. *Phys. Rev. B* **2016,** *94* (19), 195141.

(22) Müller, U., The Effective Size of Atoms. In *Inorganic Structural Chemistry*, John Wiley & Sons, Ltd: 2007; pp 45-51.

(23) Cohen, I.; Kaller, M.; Komisarchik, G.; Fuks, D.; Gelbstein, Y., Enhancement of the thermoelectric properties of *n*-type PbTe by Na and Cl co-doping. *J. Mater. Chem. C* **2015,** *3* (37), 9559-9663.

(24) Wood, C., Materials for thermoelectric energy conversion. *Rep. Prog. Phys.* **1988,** *51* (4), 459.

(25) Rowe, D. M., *Thermoelectrics Handbook: Macro to Nano*. CRC Press 2006.

(26) Biswas, K.; He, J. Q.; Zhang, Q. C.; Wang, G. Y.; Uher, C.; Dravid, V. P.; Kanatzidis, M. G., Strained endotaxial nanostructures with high thermoelectric figure of merit. *Nat. Chem.* **2011,** *3* (2), 160-166.

(27) Pei, Y. Z.; LaLonde, A. D.; Heinz, N. A.; Snyder, G. J., High Thermoelectric Figure of Merit in PbTe Alloys Demonstrated in PbTe-CdTe. *Adv. Energy Mater.* **2012,** *2* (6), 670-675.

(28) Pei, Y. Z.; Wang, H.; Gibbs, Z. M.; LaLonde, A. D.; Snyder, G. J., Thermopower enhancement in $Pb_{1-x}Mn_xTe$ alloys and its effect on thermoelectric efficiency. *NPG Asia Mater.* **2012,** *4*, 1-6.

(29) Zhao, L. D.; Wu, H. J.; Hao, S. Q.; Wu, C. I.; Zhou, X. Y.; Biswas, K.; He, J. Q.; Hogan, T. P.; Uher, C.; Wolverton, C.; Dravid, V. P.; Kanatzidis, M. G., All-scale hierarchical thermoelectrics: MgTe in PbTe facilitates valence band convergence and suppresses bipolar thermal transport for high performance. *Energy Environ. Sci.* **2013,** *6* (11), 3346-3355.

(30) Biswas, K.; He, J.; Wang, G.; Lo, S.-H.; Uher, C.; Dravid, V. P.; Kanatzidis, M. G., High thermoelectric figure of merit in nanostructured *p*-type PbTe-MTe (M = Ca, Ba). *Energy Environ. Sci.* **2011,** *4* (11), 4675-4684.

(31) Ohta, M.; Biswas, K.; Lo, S.-H.; He, J.; Chung, D. Y.; Dravid, V. P.; Kanatzidis, M. G., Enhancement of Thermoelectric Figure of Merit by the Insertion of MgTe Nanostructures in p-type PbTe Doped with $Na_2Te$. *Adv. Energy Mater.* **2012,** *2* (9), 1117-1123.

(32) Ahn, K.; Biswas, K.; He, J.; Chung, I.; Dravid, V.; Kanatzidis, M. G., Enhanced thermoelectric properties of *p*-type nanostructured PbTe-MTe (M = Cd, Hg) materials. *Energy Environ. Sci.* **2013,** *6* (5), 1529-1537.

(33) Jian, Z.; Chen, Z.; Li, W.; Yang, J.; Zhang, W.; Pei, Y., Significant band engineering effect of YbTe for high performance thermoelectric PbTe. *J. Mater. Chem. C* **2015,** *3* (48), 12410-12417.

(34) Biswas, K.; He, J. Q.; Blum, I. D.; Wu, C. I.; Hogan, T. P.; Seidman, D. N.; Dravid, V. P.; Kanatzidis, M. G., High-performance bulk thermoelectrics with all-scale hierarchical architectures. *Nature* **2012,** *489*, 414-418.

(35) Luo, J.; You, L.; Zhang, J.; Guo, K.; Zhu, H.; Gu, L.; Yang, Z.; Li, X.; Yang, J.; Zhang, W., Enhanced Average Thermoelectric Figure of Merit of the PbTe–SrTe–MnTe Alloy. *ACS Appl. Mater. Interfaces* **2017,** *9* (10), 8729-8736.

(36) He, J.; Zhao, L.-D.; Zheng, J.-C.; Doak, J. W.; Wu, H.; Wang, H.-Q.; Lee, Y.; Wolverton, C.; Kanatzidis, M. G.; Dravid, V. P., Role of Sodium Doping in Lead Chalcogenide Thermoelectrics. *J. Am. Chem. Soc.* **2013,** *135* (12), 4624-4627.

(37) Doak, J. W.; Michel, K. J.; Wolverton, C., Determining dilute-limit solvus boundaries in multi-component systems using defect energetics: Na in PbTe and PbS. *J. Mater. Chem. C* **2015,** *3* (40), 10630-10649.

(38) Kang, C.; Wang, H.; Kim, H.; Kim, S.-J.; Kim, W., Effect of Excess Na on the Morphology and Thermoelectric Properties of $Na_xPb_{1-x}Te_{0.85}Se_{0.15}$. *J. Electron. Mater.* **2014,** *43* (2), 353-358.

(39) Yamini, S. A.; Ikeda, T.; Lalonde, A.; Pei, Y.; Dou, S. X.; Snyder, G. J., Rational design of *p*-type thermoelectric PbTe: temperature dependent sodium solubility. *J. Mater. Chem. A* **2013,** *1* (31), 8725-8730.

(40) Finogenova; Popovkin, B. A.; Novoselova, A. V., Preparation of sodium telluride. *Russ. J. Inorg. Chem.* **1970,** *15*, 749-751.

(41) Böttcher, P.; Keller, R., The crystal structure of NaTe and its relationship to tellurium-rich tellurides. *J. Less-Common Met.* **1985,** *109* (2), 311-321.

(42) Finogenova, V. K.; Klimakov, A. M.; Popovkin, B. A.; Novoselova, A. V., The cross sections PbTe-$Na_2$Te and PbTe-NaTe of the system Na-Te-Pb. *Inorg. Mater.* **1971,** *7*, 1662.

(43) Blum, I. D.; Isheim, D.; Seidman, D. N.; He, J.; Androulakis, J.; Biswas, K.; Dravid, V. P.; Kanatzidis, M. G., Dopant Distributions in PbTe-Based Thermoelectric Materials. *J. Electron. Mater.* **2012,** *41* (6), 1583-1588.

(44) Kim, Y.-J.; Blum, I. D.; He, J.; Kanatzidis, M. G.; Dravid, V. P.; Seidman, D. N., Three-Dimensional Atom-Probe Tomographic Analyses of Lead-Telluride Based Thermoelectric Materials. *JOM* **2014,** *66* (11), 2288-2297.

(45) Kim, Y.-J.; Zhao, L.-D.; Kanatzidis, M. G.; Seidman, D. N., Analysis of Nanoprecipitates in a Na-Doped PbTe–SrTe Thermoelectric Material with a High Figure of Merit. *ACS Appl. Mater. Interfaces* **2017,** *9* (26), 21791-21797.

(46) He, J.; Androulakis, J.; Kanatzidis, M. G.; Dravid, V. P., Seeing Is Believing: Weak Phonon Scattering from Nanostructures in Alkali Metal-Doped Lead Telluride. *Nano Lett.* **2012,** *12* (1), 343-347.

(47) Sie, F.-R.; Liu, H.-J.; Kuo, C.-H.; Hwang, C.-S.; Chou, Y.-W.; Yeh, C.-H., Enhanced thermoelectric performance of n-type PbTe doped with Na2Te. *Intermetallics* **2018,** *92*, 113-118.

(48) Akselrud, L.; Grin, Y., WinCSD: software package for crystallographic calculations (Version 4). *J. Appl. Crystallogr.* **2014,** *47*, 803-805.

(49) Pei, Y. Z.; LaLonde, A. D.; Heinz, N. A.; Shi, X. Y.; Iwanaga, S.; Wang, H.; Chen, L. D.; Snyder, G. J., Stabilizing the Optimal Carrier Concentration for High Thermoelectric Efficiency. *Adv. Mater.* **2011,** *23* (47), 5674.

(50) Kim, H.-S.; Gibbs, Z. M.; Tang, Y.; Wang, H.; Snyder, G. J., Characterization of Lorenz number with Seebeck coefficient measurement. *Appl. Mater.* **2015,** *3* (4), 41506.

(51) Dec, S. F.; Maciel, G. E.; Fitzgerald, J. J., Solid-state sodium-23 and aluminum-27 MAS NMR study of the dehydration of $Na_2O.Al_2O_3.3H_2O$. *J. Am. Chem. Soc.* **1990,** *112* (25), 9069-9077.

(52) Nemov, S. A.; Ravich, Y. I., Thallium-doped lead chalcogenides: investigation methods and properties. *Physics-Uspekhi (Advances in Physical Sciences)* **1998,** *41* (8), 735-739.

TOC:

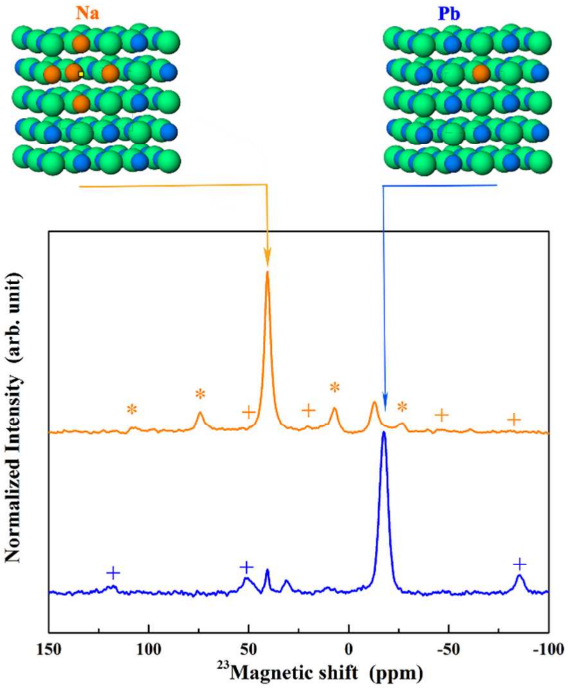
Na
Pb
Normalized Intensity (arb. unit)
150
100
50
0
-50
-100
$^{23}$Magnetic shift (ppm)

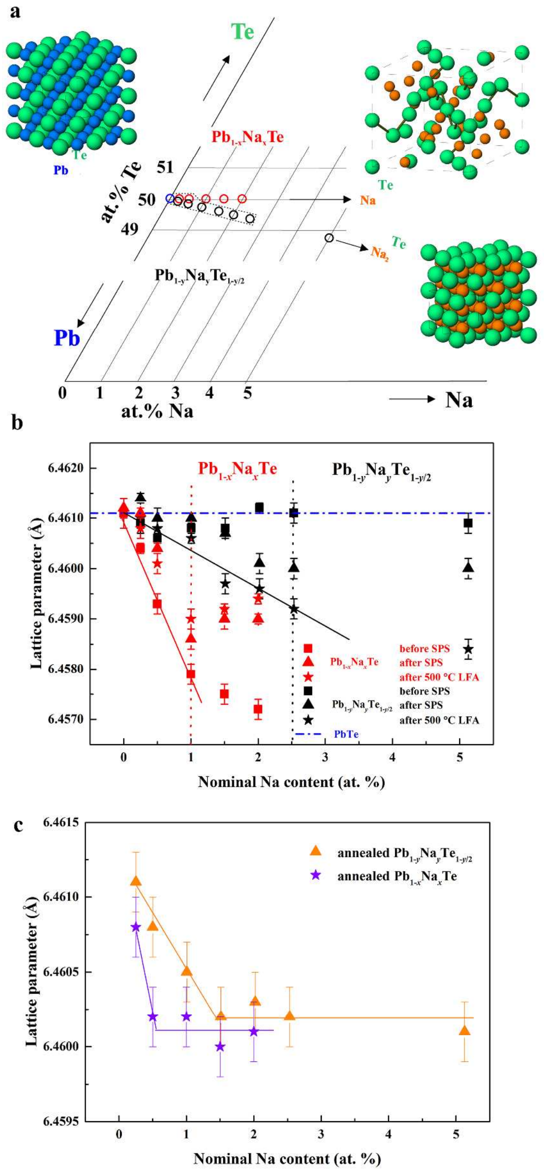

Figure 1. (a) Phase diagram for Na-substituted PbTe samples. (b) Lattice parameter vs. nominal Na composition for the $Pb_{1-x}Na_xTe$ (red) and $Pb_{1-y}Na_yTe_{1-y/2}$ (black) series. For comparison, lattice parameter of the binary PbTe is shown[14] as a blue dash dot line. (c) Lattice parameter of annealed Na-substituted PbTe samples.

150x330mm (300 x 300 DPI)

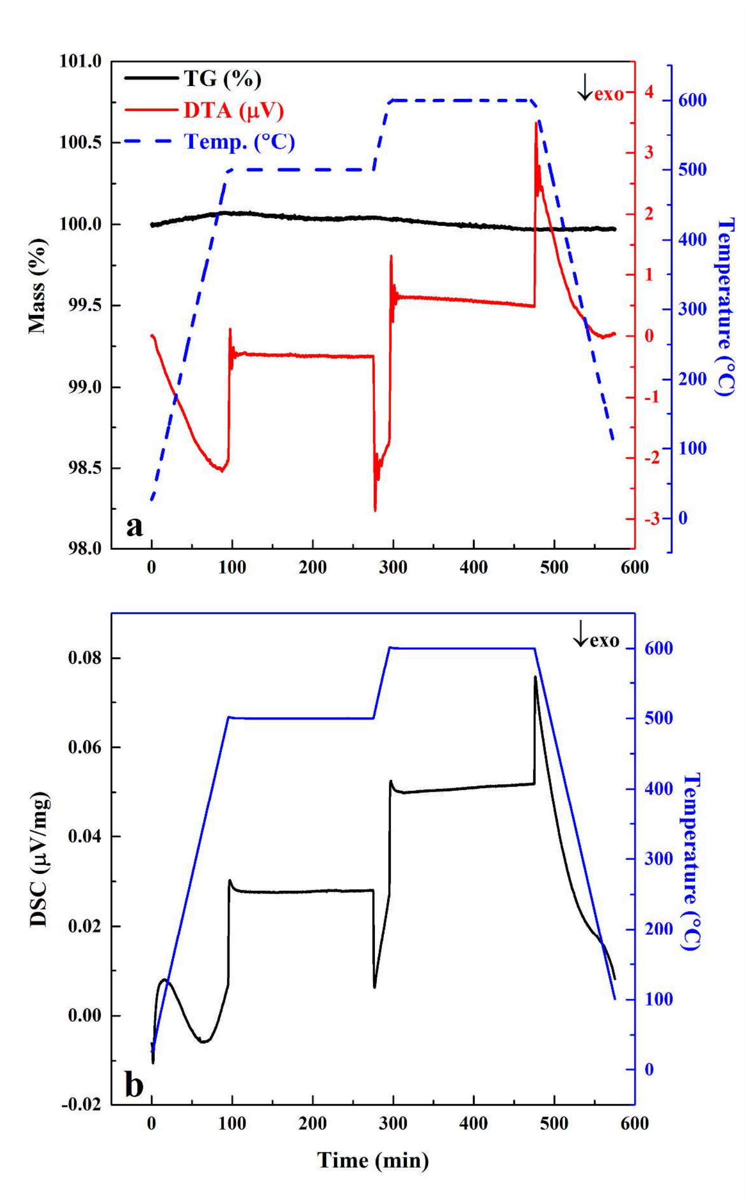

Figure 2. (a) TG / DTA measurement of $Pb_{0.98}Na_{0.02}Te$ after SPS; (b) DSC measurement of $Pb_{0.98}Na_{0.02}Te_{0.99}$ after SPS.

249x400mm (300 x 300 DPI)

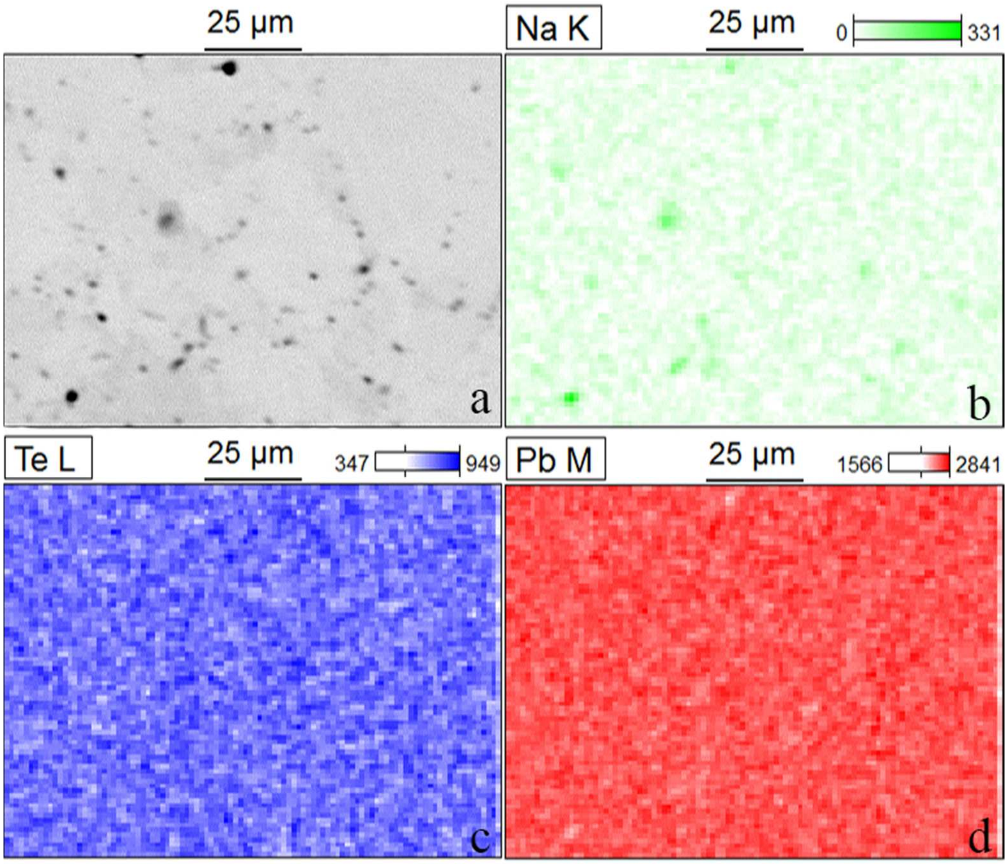

Figure 3. Back-scattered electrons (BSE) image (a) and element mapping of $Pb_{0.98}Na_{0.02}Te$ sample after SPS for (b) Na (K line), (c) Te (L lines), (d) Pb (M line).

130x114mm (150 x 150 DPI)

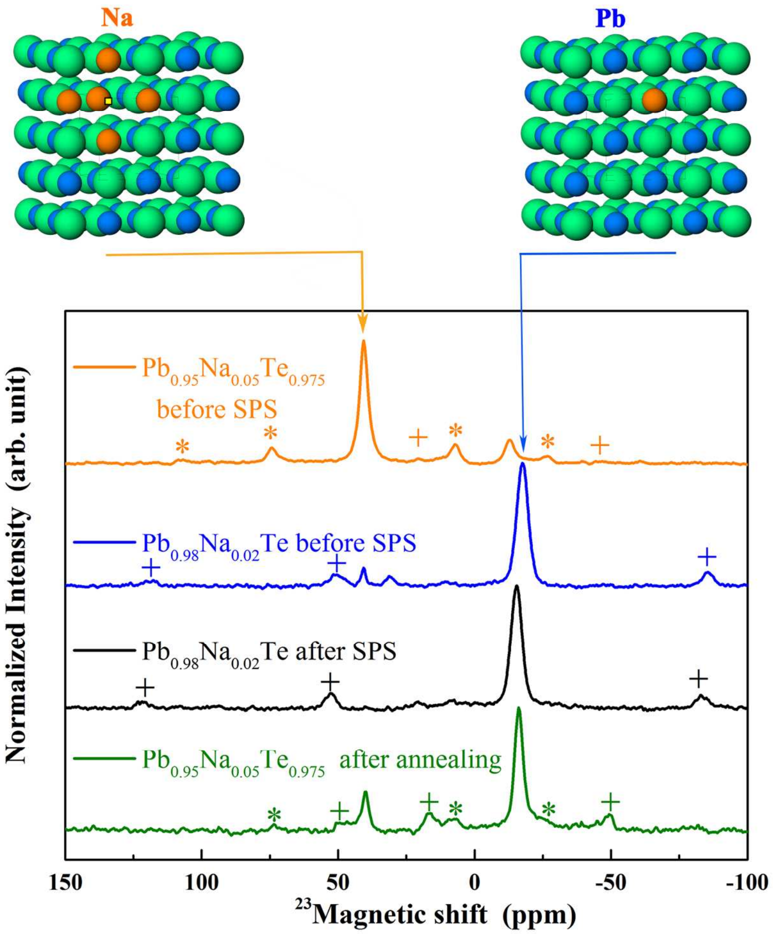

Figure 4. Magic Angle Spinning (MAS) $^{23}$Na NMR spectra of PbTe substituted with Na: (orange) $Pb_{0.95}Na_{0.05}Te_{0.975}$ after synthesis (before SPS); (blue) $Pb_{0.98}Na_{0.02}Te$ after synthesis (before SPS); (black) $Pb_{0.98}Na_{0.02}Te$ after SPS; (green) $Pb_{0.95}Na_{0.05}Te_{0.975}$ after 900 hours annealing. The spinning rate was 4.5 kHz. Spinning sidebands from the left and right signals are marked by asterisks and crosses, respectively.

160x153mm (300 x 300 DPI)

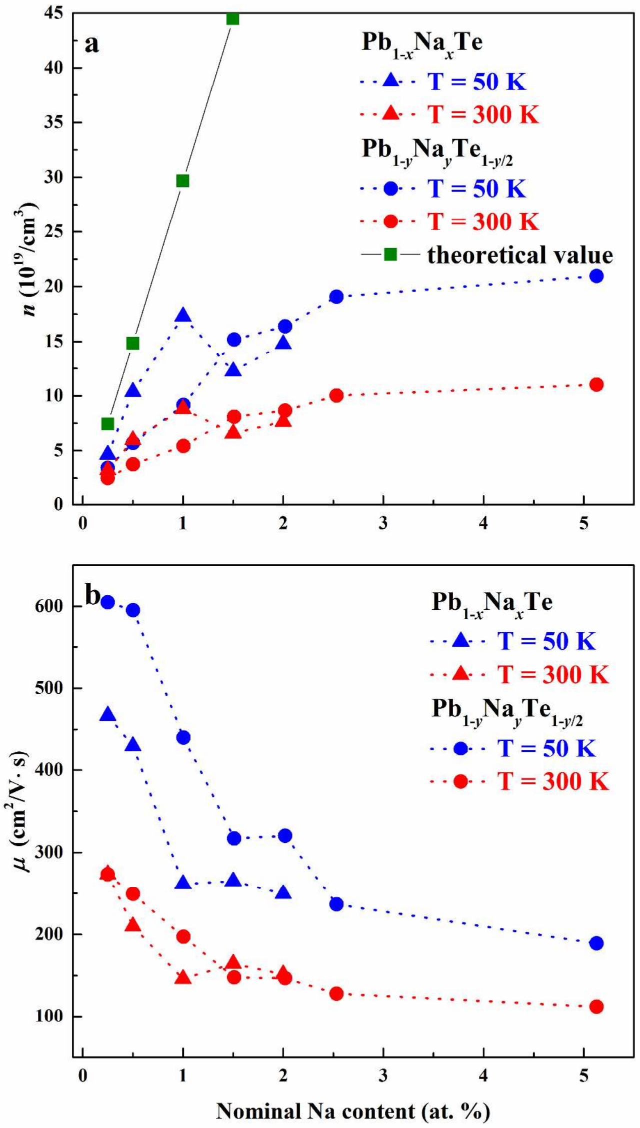

Figure 5. (a) Hall carrier concentrations and (b) carrier mobility of $Pb_{1-x}Na_xTe$ (triangles) and $Pb_{1-y}Na_yTe_{1-y/2}$ (circles) at 50 K (blue) and at 300 K (red). The calculated values (green squares) assuming one $Na^+$ donates one hole.

249x400mm (300 x 300 DPI)

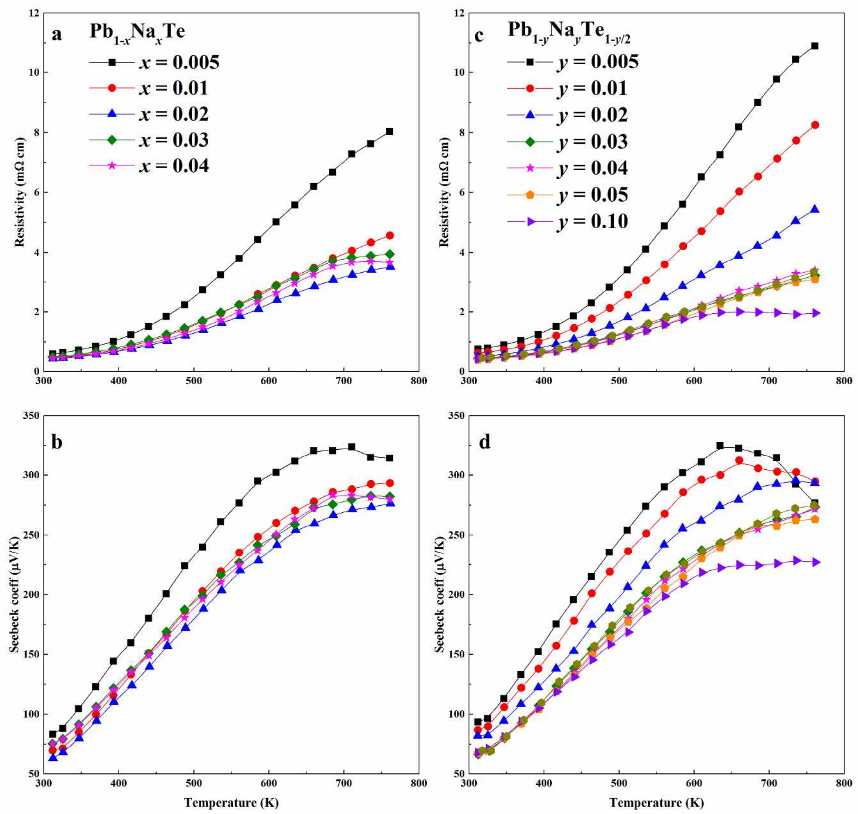

Figure 6. Temperature dependences of (a) electrical resistivity, (b) Seebeck coefficient for $Pb_{1-x}Na_xTe$ and (c) electrical resistivity, (d) Seebeck coefficient for $Pb_{1-y}Na_yTe_{1-y/2}$.

400x350mm (300 x 300 DPI)

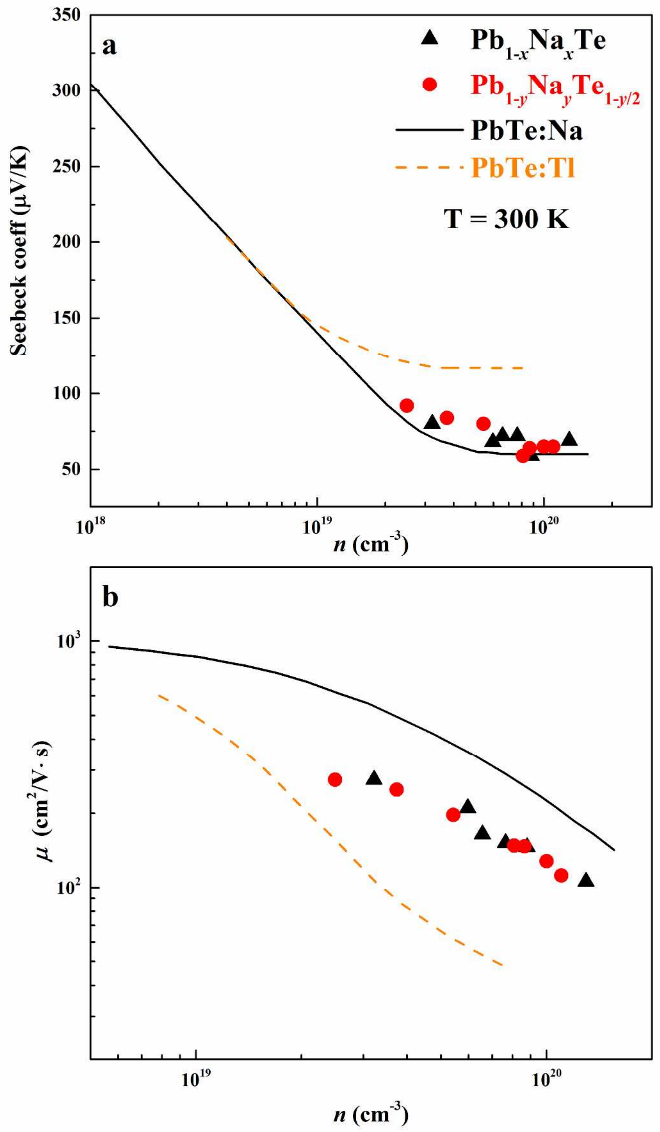

Figure 7. (a) Room-temperature Seebeck coefficient as a function of Hall carrier concentration *n* and (b) room-temperature Hall mobility *μ* as a function of Hall carrier concentration *n* for $Pb_{1-x}Na_xTe$ (triangles), $Pb_{1-y}Na_yTe_{1-y/2}$ (circles). The black and the orange lines are literature data for PbTe: Na[15, 31, 33] and PbTe: Tl[13, 28, 52], respectively.

249x400mm (300 x 300 DPI)

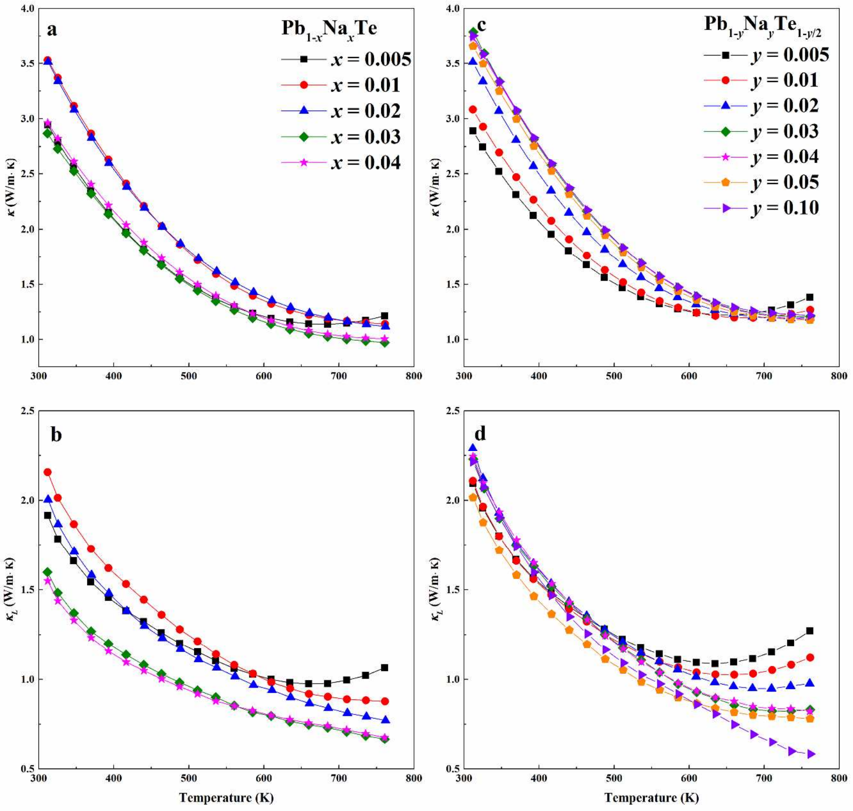

Figure 8. Temperature dependence of total and lattice thermal conductivity for $Pb_{1-x}Na_xTe$ (a, b) and $Pb_{1-y}Na_yTe_{1-y/2}$ (c, d).

400x350mm (300 x 300 DPI)

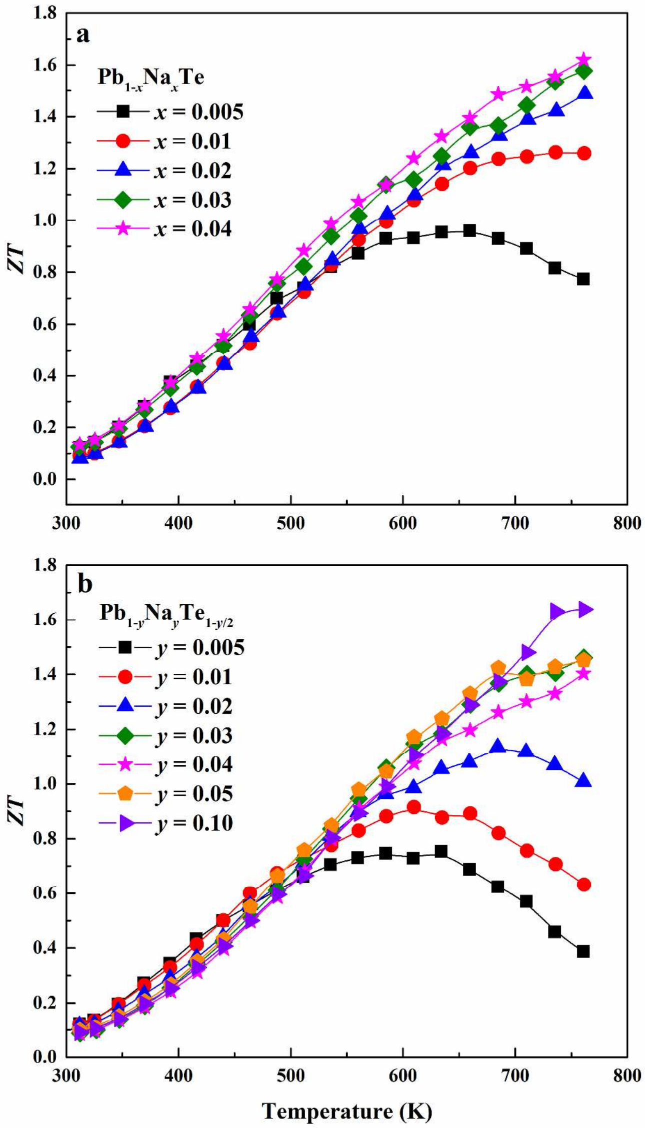

Figure 9. Temperature dependence of the thermoelectric figure of merit $ZT$ for (a) $Pb_{1-x}Na_xTe$ and (b) $Pb_{1-y}Na_yTe_{1-y/2}$.

249x400mm (300 x 300 DPI)

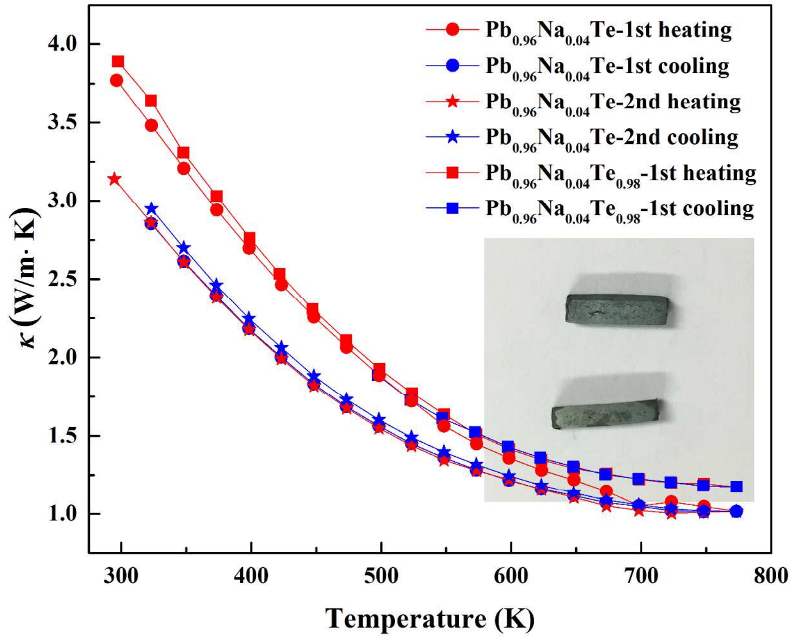

Figure 10. Cyclic measurements of thermal conductivity for $Pb_{0.96}Na_{0.04}Te$ and $Pb_{0.96}Na_{0.04}Te_{0.98}$. Inset: image of $Pb_{0.96}Na_{0.04}Te$ (top) and $Pb_{0.96}Na_{0.04}Te_{0.98}$ (bottom) specimens after measurement.

272x208mm (300 x 300 DPI)

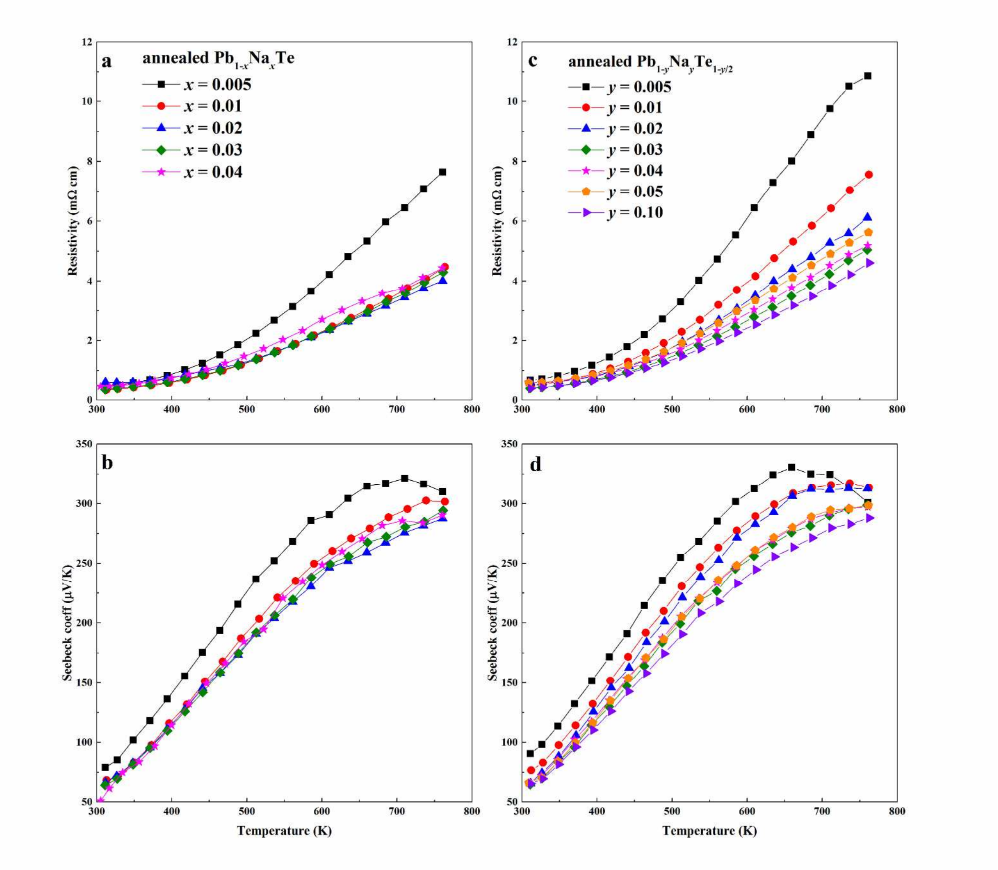

Figure 11. Temperature dependences of electrical resistivity and Seebeck coefficient for $Pb_{1-x}Na_xTe$ after 900 hours annealing at 873 K (a, b) and $Pb_{1-y}Na_yTe_{1-y/2}$ after 900 hours annealing at 873K (c, d).

400x350mm (300 x 300 DPI)

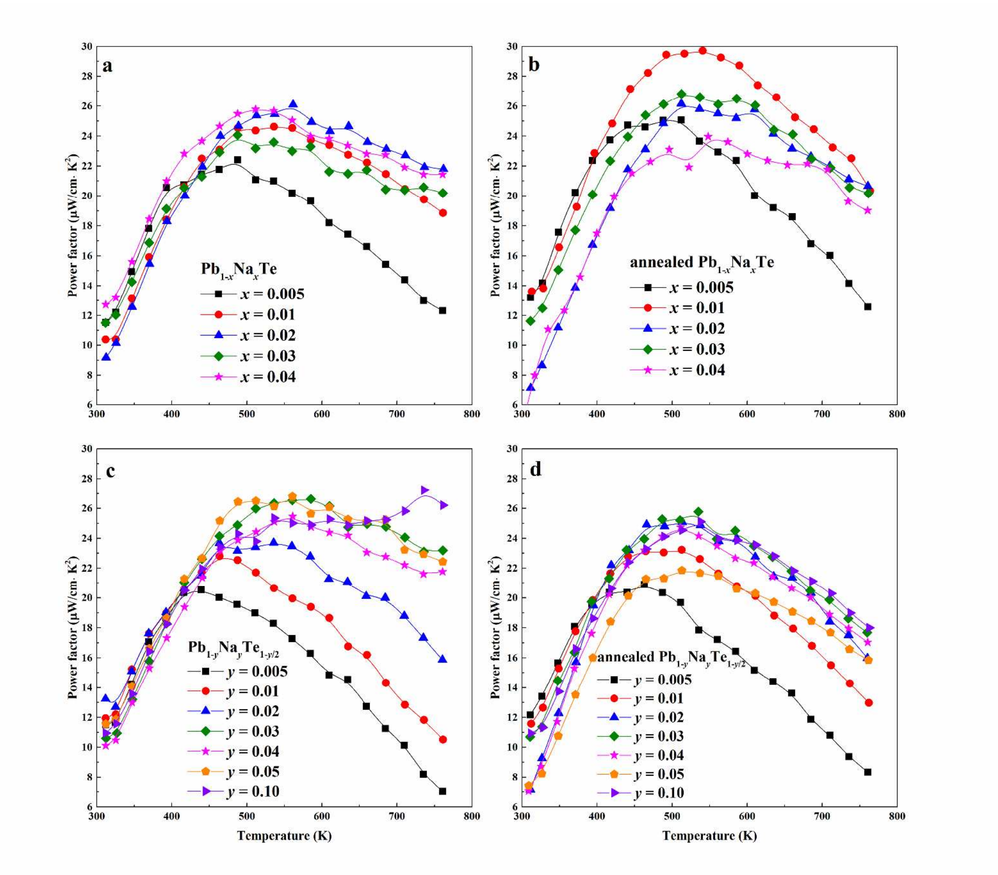

Figure 12. Temperature dependences of power factor for $Pb_{1-x}Na_xTe$ before (a) and after (b) 900 hours annealing at 873 K and for $Pb_{1-y}Na_yTe_{1-y/2}$ before (c) and after (d) 900 hours annealing at 873 K.

400x350mm (300 x 300 DPI)

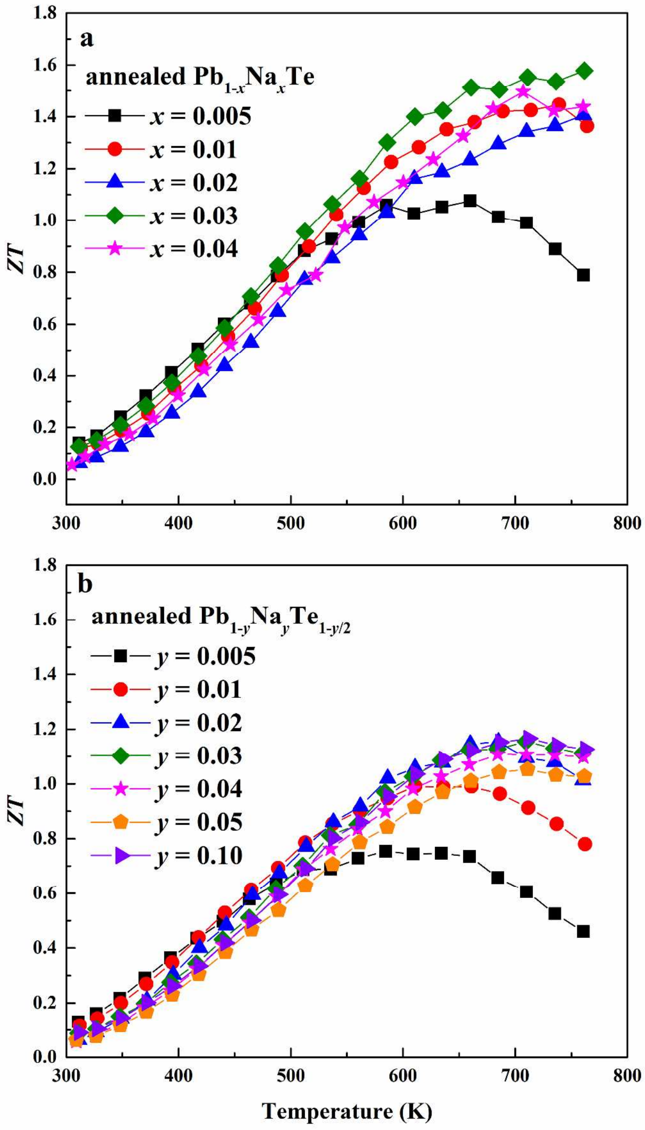

Figure 13. Temperature dependent of the thermoelectric figure of merit *ZT* for (a) $Pb_{1-x}Na_xTe$ and for (b) $Pb_{1-y}Na_yTe_{1-y/2}$ after 900 hours annealing at 873 K.

249x400mm (300 x 300 DPI)